ELSEVIER

Nuclear Instruments and Methods in Physics Research B 175–177 (2001) 1–11

NIM B
Beam Interactions with Materials & Atoms

www.elsevier.nl/locate/nimb

Energy dissipation of fast heavy ions in matter

G. Schiwietz [a,*], E. Luderer [a], G. Xiao [a], P.L. Grande [b]

[a] *Hahn-Meitner-Institut, Bereich Festkörperphysik, Glienicker Str. 100, 14109 Berlin, Germany*
[b] *Instituto de Fisica, Universidade Federal do Rio Grande do Sul, 91500 Porto Alegre, Brazil*

Abstract

The energy dissipation due to fast heavy ions in matter is critically reviewed with emphasis on possible mechanisms that lead to material modifications. Starting from a discussion of the initial electronic energy-deposition processes, three basic mechanisms for the conversion of electronic into atomic energy are investigated. Experimental evidence for a highly charged track region as well as for hot electrons inside tracks is presented. As follows mainly from Auger-electron spectroscopy, there are strong indications for different track-production mechanisms in different materials.

1. Introduction

Fast heavy ions may lead to permanent material changes in a small cylinder along the nearly straight ion path, giving rise to the so-called ion tracks. The appearance of track effects in polymers is known since some decades [1] and has found widespread applications in the meanwhile [2]. Nowadays it is known that other insulators and even metallic glasses [3] are also subject to materials modifications by heavy ions. There are, however, a few contradictory models for the track-production mechanisms and until now most of them cannot completely be ruled out. In order to point out what are the weaknesses of our present knowledge, a short review of the possible scenarios of the track evolution is given. Special emphasis is devoted to the short-time phenomena from the initial ion-energy loss processes to the electronic de-excitation processes.

The first step of the nuclear-track evolution is the ionization and excitation of atoms close to ion path. The most important parameters that drive subsequent solid-state reactions are the *local electron-energy density* and the *local ionization density*, as will be explained below. Current experimental techniques do not have direct access to these quantities. The closely related *total ion-energy loss* and the degree of *inner-shell ionization*, however, are subject to many investigations and they are discussed in Section 2 for the case of fast heavy ions.

After the initial energy-transfer by heavy ions, the center of the track is highly ionized. Then it depends on the ionization density and on the *charge-neutralization time* whether the mutual repulsion of target ions may convert a significant

* Corresponding author. Tel.: +49-30-8062-24-48; fax: +49-30-8062-22-93.
E-mail address: schiwietz@hmi.de (G. Schiwietz).

0168-583X/01/$ - see front matter
PII: S0168-583X(00)00544-9

amount of electronic potential energy into atomic motion. This conversion mechanism is described by the Coulomb-explosion model [1,4–6] and the corresponding electrostatic potential is discussed in Section 3. Coulomb explosion will be significant only if the charge-neutralization time exceeds 10^{-14} s for light target atoms. Theory, however, predicts neutralization times of about 10^{-16} s for free-electron gas like metals, such as Al.

Thus, for many metals charge neutralization is too fast and Coulomb explosion is impossible. In this case, however, electronic recombination might still be slow, leaving a hot electron gas at the center of the track. Two different mechanisms may then convert this electronic energy (quantified by an *electron temperature*, as discussed in Section 4) into atomic motion.

- The lattice-relaxation model [7–9] describes a collective atomic rearrangement due to (predominantly repulsive or antibinding) non-equilibrium potentials. Thus, a fraction of the electronic potential energy, or equivalently the degree of target excitation, leads to modified *inter-atomic forces* and subsequent atomic motion in this model.
- The thermal-spike model [10–15] assumes that electronic excitation leads, via the electron–phonon coupling (equivalent to electron–atom collisions), to an increased atomic motion. Thus, except for the efficiency of the *electron–phonon coupling*, the kinetic electron energy is the main ingredient in this model.

The relative importance of the three models depends on the charge-neutralization time, on the strength of the modified inter-atomic forces and on the electron–phonon coupling constant. For highly excited ion tracks, all these quantities are unknown and, thus, the influence of a certain mechanism can only be determined experimentally. This, however, is complicated by the fact that atomic motion in solid matter may be converted into a stochastic motion on a time scale of 10^{-13} to 10^{-12} s, independent of the early stage of the evolution. Furthermore, slow atomic relaxation processes, such as recrystallization, and the influence of local structures and delay times on phase transitions may prohibit any definite conclusions. Hence, there seems to be no way to decide between the models on a pure experimental basis, if only modified material properties are investigated.

One possible way to improve the interpretation of material modification effects is the investigation of prompt emitted 'particles' that carry information from inside the track. Ejected electrons or X-rays can be used as precursors of the corresponding transient material states. Electrons may be probes for the first 10^{-18} to 10^{-14} s of the track formation and energy dissipation. For reviews on transport of fast electrons and fast-ion-induced electron emission from solids, the reader is referred to [16–19].

In this work, we concentrate only on the solid-state interactions of fast ions (very fast compared to the Fermi velocity, or equivalently $\gg$25 keV/u) close to their equilibrium charge state. We will be concerned with projectiles at energies per mass unit of $E_p/M_p = 2$ to 5 MeV/u, corresponding to about 10% the speed of light, where the nuclear energy loss is only a minor fraction of the total ion energy loss. Inside thin foils these ions serve as a nearly instantaneous source of excitation along their trajectory. They do neither change their charge state significantly nor their energy or direction of motion. Thus, they excite and they probe the target without being significantly perturbed during the penetration.

2. Ion energy-loss and target ionization

In this section, the initial excitation processes will be discussed. An approximate determination of the strength of such processes is possible from the investigation of the projectile energy loss and of multiple inner-shell ionization. We may ask the question "How is the energy dumped into the solid and what fraction of the total energy is responsible for track effects?".

Low-energy ions slow down due to a manyfold of different processes, strongly dependent on the projectile charge state and on the specific projectile–target combination. These processes are the nuclear energy transfer, electron capture, excitation and ionization of target as well as projectile electrons. For few electron systems (H + H or H + He), there exist accurate quantum-mechanical

solutions of the time-dependent Schrödinger equation, yielding stopping powers that agree to within a few percent with the experimental data. The remaining discrepancies may even be traced back to result from the neglect of electron-correlation effects [20–22]. Also impact-parameter dependent ionization probabilities and electronic energy transfers are in reasonable agreement with the available experimental data [23]. The situation is less satisfying for many electron systems as they are typical for ion–solid interactions. However, the whole treatment simplifies again if we restrict ourselves to fast projectiles.

Fast ions loose their kinetic energy mainly through ionization of atoms from all shells and to some extent through excitation of valence- and conduction-band states. Although the current experimental uncertainties of energy-loss determinations are much below the theoretical uncertainties, these energy-loss mechanisms are expected to be qualitatively well understood. Different attempts for a precise description of the energy loss of swift ions in multi-electron targets are currently being worked out [24–29].

Fig. 1 displays such specific energy-loss results for H, N, S, Ag and U ions in amorphous carbon (a-C) as a function of the projectile energy. The experimental data for N and S at low energies as well as the ones for hydrogen projectiles have been taken from the data collection by Paul [30]. The other data at 5 MeV/u have been taken from [31–33]. The TRIM results [34] are fits to the similar experimental data sets and correspondingly there is a good agreement. At 5 MeV/u one may compare the electronic energy loss (S_e) or the total energy loss with the quasi-elastic nuclear contribution (S_n). It is seen that S_n is about three orders of magnitude lower than S_e. Hence, the electronic energy loss is completely dominating the energy-transfer processes.

At energies above 100 keV/u the results of the unitary convolution approximation (UCA) agree to within about 10% with the experimental data. For heavy ions, these ab initio quantum results appear even to be superior over the multi-parameter fits (TRIM91). The UCA for bare ions is basically an impact-parameter dependent version of the non-perturbative Bloch theory of slowing

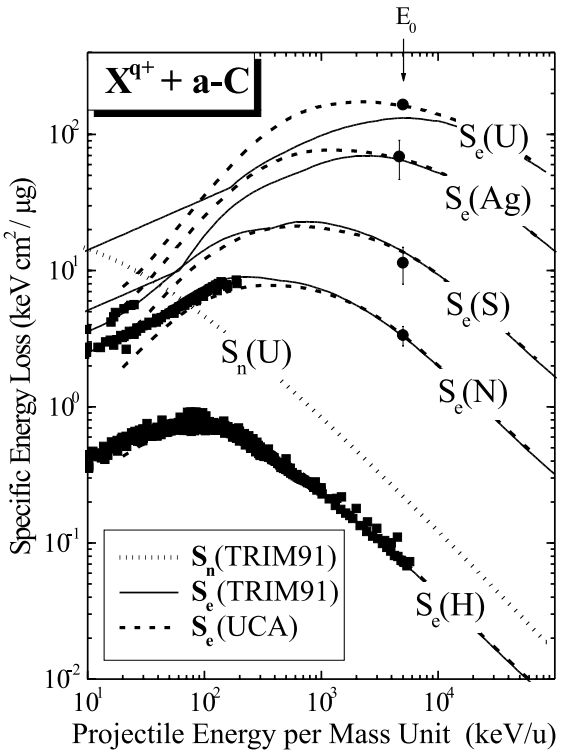

Fig. 1. Energy dependence of the energy loss of various ions in a-C. Experimental data are shown as solid symbols. TRIM91 results for the electronic S_e and nuclear energy loss S_n are shown as dotted and solid curves. Current quantum ab initio results for S_e based on the UCA model are shown as dashed lines.

down. The UCA does rigorously neglect all target-polarization terms (Barkas effect and collective screening), which leads to uncertainties of about 10% at high velocities. It makes use of explicit projectile-screening functions and of numerical target-electron densities. Thus, it yields the initial energy deposition as a function of the distance from the track, a quantity that directly enters the lattice-relaxation and thermal-spike models. Hence, nowadays there are energy-loss models available that are more accurate than most other ingredients of the track models.

The energy loss due to ionization may always be decomposed into a mean transferred energy and an impact-parameter dependent ionization probability $P(b)$. The ionization probability is one of the central parameters of the Coulomb-explosion

model. Using Auger-electron or X-ray spectroscopy one may determine the degree of multiple ionization of inner shells from the fractional hypersatellite intensities. Hypersatellite lines result from multiple inner-shell vacancies that reduce the screening and increase the Auger transition energies. As an example, double K-shell ionization of carbon atoms in different matrices will be considered here.

Fig. 2 displays the ratio of double to single ionization events corresponding to the interaction of different particles, from incident electrons to highly charged U ions, in their equilibrium charge state. The data have been extracted from Auger-line intensities, considering electron escape depths, Auger cascades, and δ-electron collision cascades. The theoretical curves are quantum results calculated for bare ions at 5 MeV/u in the first-order perturbation theory (FO) and in the so-called Magnus approximation.

Previous data for a-C [35–37] are shown as open symbols (squares). New results for diamond-like carbon (DLC supplied by Schultrich et al., plotted as solid diamonds) as well as for highly oriented pyrolytic graphite (HOPG, plotted as solid circles) have been taken for 5 MeV/u Ar^{16+} and 2 MeV/u Kr^{24+} ions. All new data points have been obtained with a new ultra-high vacuum setup (this setup will be described in detail in a subsequent paper) ensuring low surface contaminations. As expected, the K-shell double ionization ratio

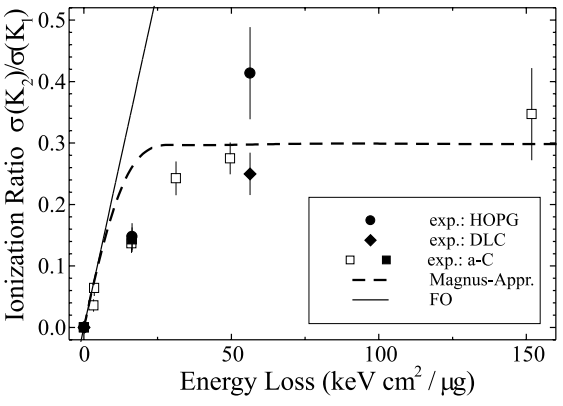

Fig. 2. Ratio of double to single ionization cross-sections versus the projectile energy-loss (see text).

does not significantly depend on the structure (amorphous versus crystalline solids or diamond-like versus graphite-like bonds) of the carbon target. Only one data point for 2 MeV/u Kr^{24+} on HOPG appears to lie somewhat outside the general experimental trend.

In an independent electron model (IEM) within first-order perturbation theory (FO), one expects the ratio R to be roughly proportional to the electronic stopping power S_e. This is not the case, as can be seen from the results in Fig. 2. For the heavy ions Ni, Kr and U with high energy losses there is a clear saturation of R. The dashed curve in the figure is a theoretical result, calculated within the Magnus approximation [22] for numerical wave functions being eigenstates of a spherically averaged solid-state potential. It is still based on the IEM, but goes beyond the perturbation theory. There is a qualitative agreement between these theoretical results and the data, the saturation values being the same.

The ionization probabilities in the Magnus approximation are close to 100% for heavy ions at small impact parameters (they exceed 100% by far in the first-order perturbation theory). Exactly this restriction of ionization probabilities to $\leqslant$100% leads to the saturation observed in Fig. 2. The overestimated double-ionization cross-sections for small q are due to the neglect of dynamic screening and electron correlation in the double ionization process. Taking this failure of our model results into account, we estimate that there is *complete ionization of the K-shell as well as the valence band of carbon* in central collisions with projectiles exceeding about 25 keV $cm^2/\mu g$.

3. Nuclear-track potential and Coulomb explosion

Strong ionization of atoms close to the ion track leads to a positive nuclear-track potential which is possible to detect if the charge neutralization is slow enough. This potential does not act on emitted photons, but it decelerates emitted electrons. Line structures in the electron spectrum (the convoy electron peak or Auger lines) may be used to determine this deceleration. In fact, a deceleration of convoy electrons (these electrons

move approximately with the projectile speed in the projectile direction) as well as of Auger electrons has been found for the insulators polypropylene (PP, C_3H_6) as well as mylar and will be discussed in the following.

For the key point of this investigation, the measurement of electron energy-spectra, two electrostatic electron spectrometers were used. For the determination of zero-degree electron spectra (ejection in beam direction) a tandem spectrometer was used, where the primary beam can pass through the first stage of the analyzer. The measurement of target Auger-electron energy distributions was performed with a single-stage parallel-plate spectrometer at an ejection angle of 135°. The uncertainty of the energy calibrations is about ±0.5 eV.

Most experiments with insulators were performed with polypropylene (PP, $[C_3H_6]_n$) foils at thicknesses of 0.5 and 1.5 μm. An Auger-spectroscopic surface analysis showed that the PP samples have a 5% O contamination, leading only to minor uncertainties for the present investigation. Two serious problems, however, exist for insulating foils: beam-induced melting and evaporation due to the low heat conductivity and also macroscopic charging due to the low electrical conductivity. We have solved both problems by evaporating a conducting film on one side of the sample. For the results presented in this work we have used Al coatings of 20 and 30 μg/cm^2 and for the PP substrate we expect a maximum temperature rise of less then 50 K for the highest ion flux during the irradiation.

The effects of macroscopic charging are easy to observe for electron irradiation. Within some minutes the target-Auger lines were shifted to higher energies by up to a few hundred eV. When the shift was approaching a breakthrough voltage, it was suddenly reduced and the charging-up process was repeated with a breakthrough time inversely proportional to the incident electron current. This effect was also observable as a fluctuation of the target current. In contrast to the electron measurements, we found no such indications for charging up in the case of heavy-ion irradiation at the same incident velocity. Here we found sharp Auger- and convoy-line structures and no significant dependence of the target/beam current ratio on the beam current. This allows us to put an upper limit of about 3 V on *fluctuations* and about 20 V on the *absolute value* of a surface potential due to macroscopic charging ΔV_{mac} in PP. In fact, ion tracks seem to act as shortcuts that limit the charging.

The low-energy electron spectra, however, indicate a shift of the continuous spectral structure toward lower energies in the case of low fluences. With increasing fluence this shift vanishes, since the foils loose hydrogen during irradiation, the so-called carbonization process. At the highest fluences investigated in this work, the relative hydrogen contents is reduced from 66% to below 50% [38,39]. This leads to an increased conductivity and reduced recombination times, as can be seen from the Auger- and convoy-electron spectra as well as from DC-resistivity measurements. It is emphasized that the electrons at energies below about 50 eV are mainly created via electron–electron collision cascades [40,41] and penetrate the surface further away from the ion path (typically 20–100 Å). Thus, the electron spectrum close to zero energy will predominantly be influenced by macroscopic surface potentials and less efficiently by any microscopic track effect.

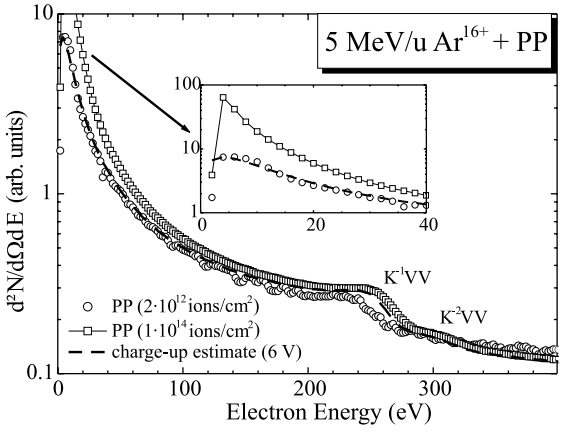

Fig. 3. Experimental low-energy electron spectra for 5 MeV/u Ar^{16+}-ions on PP measured under a backward angle of 135° for two different fluences. The carbon KVV-Auger structures for single ($K^{-1}VV$) and double K vacancies ($K^{-2}VV$) are also visible. The dashed curve is explained in the text.

Fig. 3 displays this low-energy part of the first (circles) and the last (squares) spectrum of a series of measurements taken for 5 MeV/u Ar^{16+} projectiles with the same 1.5 μm PP sample. The fluence differs by about two orders of magnitude between the two measurements. The low-energy part below about 20 eV shows a strong increase with increasing fluence (see the inset in Fig. 3) and the final spectrum is similar to the one for a-C (not shown in the figure). One may transform the singly differential energy distribution $dN/dE(E)$ for a sample without macroscopic fields (the high-fluence case) into a spectrum $dN'/dE(E)$ under the influence of a positive surface potential ΔV_{mac} (the low fluence case) using

$$dN'/dE(E) = dN/dE(E) \times E/[E + \Delta V_{mac}],$$

where E is the electron energy with respect to the vacuum level. Here we have assumed that chemical changes of the sample do not influence the spectrum inside the solid and that the macroscopic field between sample and spectrometer gives rise to refraction at a planar potential [17]. The dashed line in the figure shows the result of this transformation, where the experimental high-fluence data are transformed using $\Delta V_{mac} = 6$ V. Below an energy of about 100 eV there is a good agreement of this curve with the low-fluence spectrum.

At energies of about 260 and 310 eV, there are structures superimposed on the continuous spectrum in Fig. 3. These structures are due to target KVV-Auger electrons (here K stands for a K vacancy and each V stands for a valence-band electron that is either emitted or transferred to an empty K level during the Auger decay). The Auger structures are shifted by about 22 eV between both measurements. As discussed above, 6 eV are due to macroscopic charging and the remaining 16 eV are due to a microscopic effect. The latter contribution to the shift is produced by the nuclear-track potential [38,39], i.e., by the positive charges of the atomic cores at the center of the track. For Ar^{16+} ions or heavier projectiles, however, there is a significant ionization of the valence band. Hence, prompt Auger decay is impossible and the measured energy shift is representative for a partially neutralized track. The full track potential can only be determined with lighter ions such as N or Ne, since for these ions there exist more than two valence electrons per atom and fast Auger decay is possible. Correspondingly, for N^{7+} and Ne^{9+} ions at 5 MeV/u we have determined much larger track potentials of 20.5 and 42 eV [38,39].

Comparison with theory shows that these measured potentials are close to the maximum expected value, indicating that there is no significant recombination during the Auger decay time of about 1.1×10^{-14} s. Quantitative estimates indicate that the track lifetime is $>1.5 \times 10^{-14}$ s. Thus, for heavy ions, the nuclear-track potential in PP is strong enough and it survives long enough to allow at least for a partial Coulomb explosion. For other carbon structures, such as amorphous diamond-like and graphite-like carbon as well as crystalline graphite, energy shifts are below 2 eV. Thus, recombination is much faster in these materials and Coulomb explosion is impossible.

Alternative to the Auger analysis it is also possible to investigate the track potential using the so-called convoy electrons. At an electron ejection angle of 0° with respect to the beam and for a velocity equal to the projectile speed a cusp-shaped peak appears in the spectrum of the ejected electrons. This peak is due to capture and also loss of electrons into low-lying continuum states of the projectile. Both processes have been investigated intensively for gas targets and a similar peak, named convoy-electron peak, was also found for solid-state targets.

Fig. 4 shows the peak energy of convoy electrons for 5 MeV/u Ni^{23+} ions penetrating PP-foils with the evaporated Al layer in beam direction (squares) and opposite to the beam direction (circles). Two different samples have been used for each of the two geometries and the accuracy of the energy determinations is about 2 eV. It is seen that the energy of the convoy peak increases with increasing fluence. For the upper curve our measured convoy-energy is consistent with the final projectile velocities obtained by using a surface-barrier detector (except for a constant convoy-energy increase by about 5 eV due to the projectile-image charge). Carbonization of the PP foil leads to a reduction of the foil thickness and correspondingly to a reduced projectile energy-

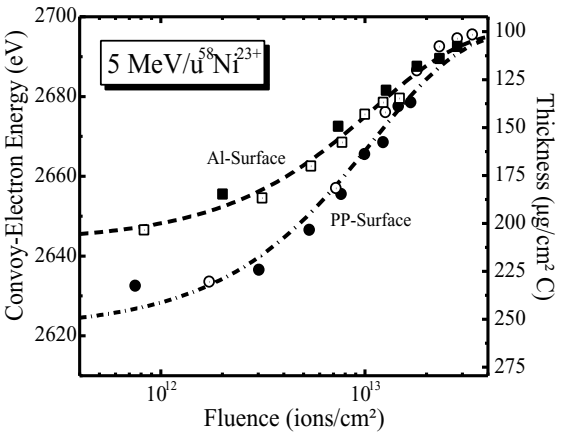

Fig. 4. Peak energy of convoy electrons for 5 MeV/u Ni^{23+} + PP-foils versus fluence. The upper data set (squares) was taken for the Al coating and the lower data set (circles) for the PP surface pointing towards the 0°-spectrometer. The curves are fits to the data.

loss. This gives rise to increased projectile energies and convoy-electron energies [42].

The lower curve, however, is influenced by additional solid-state potentials that vanish in the limit of high fluences. This behavior is determined by the electron-recombination properties of PP, which change drastically with fluence, again as a result of carbonization. In the limit of low fluences, however, we find an influence of the track potential. After subtracting offsets due to macroscopic charging and due to image potentials from the energy difference of both curves in Fig. 4, there is a remaining deceleration of about 8 eV due to the track potential. A fraction of convoy electrons (roughly 50%) travels behind the projectile and only these electrons are subject to a deceleration [42]. Since the attractive projectile potential tries to keep the convoy electrons at the projectile speed, the measured shift should always be significantly smaller than the full nuclear-track potential.

In contrast to the PP results, we find accelerated convoy electrons for amorphous graphite-like carbon (a-C) due to the negative projectile-image charge. Thus, the recombination inside the track must be very fast in this material. Quantitative estimates indicate that the track lifetime is $<4 \times 10^{-16}$ s in a-C.

As discussed above, in PP we expect a significant influence of Coulomb explosion on the material properties. Indications for a weak influence of the corresponding track potential on the energy spectrum of desorbed H_n^+ ions from hydrocarbons have been reported previously [43]. For the PP targets this may be investigated further by a determination of absolute desorption (erosion) yields for different incident ions. Using fluence dependences as in Fig. 4, we have determined the erosion yields from the initial slope and the total energy loss inside the foils as well as from the saturation fluence. The results of both methods agree to within about 30%.

Fig. 5 displays the corresponding desorption cross-sections for five different projectile ions. For comparison we have also included a simple estimate for the valence-band ionization (curve labeled primary bond-breaking) using the first-order quantum perturbation theory. Furthermore, an estimate for the total number of broken bonds is derived from the ratio of the total energy-loss cross-section and an averaged energy of the bonds (curve labeled total bond-breaking). First we note that the experimental data are completely inconsistent with primary bond-breaking by the incident projectile. Furthermore, the experimental data are consistent with an S_e^2 proportionality for low atomic numbers Z_p and they are proportional to S_e for high projectile atomic numbers, where they

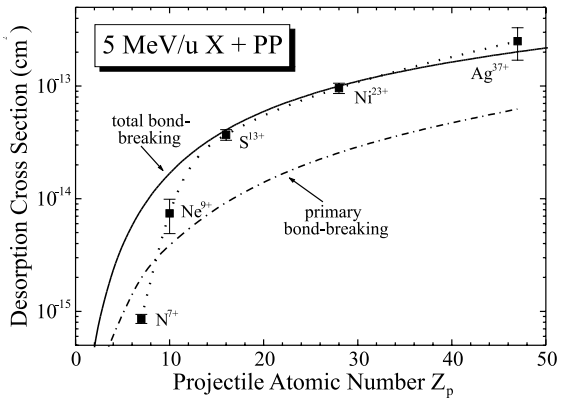

Fig. 5. Erosion cross-sections as determined from the fluence dependent energy loss in comparison with simple estimates for bond breaking (see text).

join the total bond-breaking curve. This indicates that there is a threshold-behavior for $Z_p \approx 13$. Additionally, this proves that a large fraction of the total deposited energy is converted into broken bonds for $Z_p > 15$. Both facts are consistent with the Coulomb-explosion model, as there are ionization probabilities of >60% for all electrons in the center of the track (see also Fig. 2) and nuclear-track potentials of >70 eV for $Z_p > 15$ at 5 MeV/u. At least all ionized hydrogen atoms close to the track will be set in motion by such a strong track potential.

We have also investigated the erosion of PP using mass spectrometry and previously with an in situ nuclear reaction method. Both techniques yield a ratio of about 1/6 for the number depleted carbon atoms divided into the number of ejected hydrogen atoms. From the knowledge of the fractional stopping powers of H and C, one may estimate that the erosion stops when the target is converted from C_3H_6 to $C_{2.1}H_{0.6}$. At this stage the energy loss inside the foil is reduced to 50% of its initial value. Using the absolute numbers from Fig. 5, we estimate initial erosion yields of 5×10^5 *ejected C atoms and* 3×10^6 *H atoms per incident* Ag^{37+} ion. These numbers reduce if the 1.5 μm PP foils are replaced by thinner foils of 0.5 μm. Thus, these extraordinary high erosion yields are due to an outgassing from deep inside the samples.

4. Electron temperatures, thermal spike and lattice relaxation

As we have shown in Section 3, graphite-like amorphous carbon (a-C) and DLC as well as highly oriented pyrolytic graphite (HOPG) are subject to strong initial ionizations by heavy ions. But these materials do not show significant nuclear-track potentials and correspondingly Coulomb explosion is impossible. In this section we will discuss the possibility of the thermal spike and lattice relaxation as a result of highly excited track cores after neutralization. Experimental data for the electron temperature after neutralization, the main ingredient of both models, are presented and compared with the theoretical estimates.

So far, we have investigated the intensity (see Fig. 2) and the shift of Auger lines (see Fig. 3). But the slope of the Auger lines carries information about the degree of excitation of the valence band during the K decay. The high-energy shoulder of the Auger structures reflects a convolution of the populated density of states near the Fermi level [44,45]. This population density should be well described by a Fermi–Dirac distribution [46–48]. As described in detail in previous publications [35–37] the line widths increase with increasing projectile charge-state, or with increasing electron temperature. The data evaluation are based on a comparison with the Auger spectra for incident electrons. First we fit these spectra using a simple model for electron transport [49] that includes the density of states, assuming that the corresponding electron temperature in the valence band is virtually zero. Electron temperatures are then extracted from fits to ion-induced spectra, by a variation of the Fermi–Dirac distribution and by keeping all other transport properties fixed.

Fig. 6 displays electron temperatures for two different Auger decay times, corresponding to single (closed symbols for $\tau_{K^1VV} = 11 \times 10^{-15}$ s) and double (open symbols for $\tau_{K^2VV} = 6 \times 10^{-15}$ s) K-vacancy states. Theoretical curves calculated for decay times of 6 and 11 fs and ions at 5 MeV/u in a-C are shown for comparison [35–37]. This model

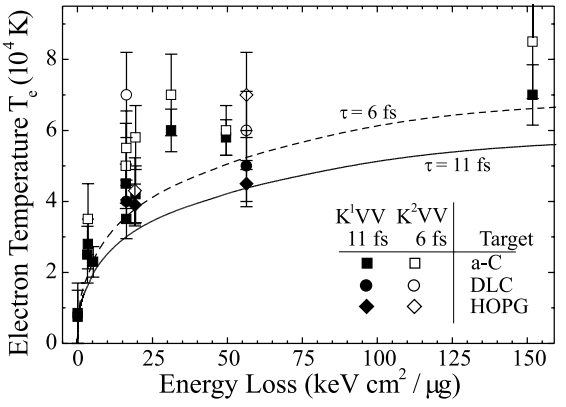

Fig. 6. Electron temperatures as determined from the broadening of two Auger lines for three C modifications and different projectile species in comparison with the model calculations (see text).

includes the impact-parameter distribution of the initial energy deposition as well as an estimate for the transport of fast electrons and for the influence of Auger processes on the valence-band temperatures. The time dependence of the electron temperature is then calculated from the heat diffusion equation using ab initio values for the electronic transport properties.

Previous data for graphite-like a-C [35–37] have been supplemented by three additional data points. First results for DLC (DLC supplied by Schultric et al., plotted as diamonds) as well as for HOPG (HOPG, plotted as circles) have been taken for 5 MeV/u $Ar^{8+,16+}$ and 2 MeV/u $Kr^{12+,24+}$ ions. Note that we have also included ions with non-equilibrium charge-states (Ar^{8+} and Kr^{12+}) in this plot. The present results have been taken with a new ultra-high vacuum setup. The residual-gas was dominated by H_2 with total pressures between 10^{-10} and 10^{-9} mbar during the different beam times. The HOPG samples were cleaved and the DLC samples were heated to about 500 K prior to the final measurements. For both target types we have observed beam-induced desorption, leading to negligible O surface coverages after some minutes of irradiation.

The experimental as well as the theoretical data points show a slow increase as a function of the electronic energy loss. For high projectile energy-losses electron temperatures of about 80 000 K are reached. The experimental results exceed the theoretical predictions by about 35% on the average. The relative energy dependence and the temperature ratio for 6 and 11 fs agree very well between theory and experiment. Thus, it seems as if these high electronic excitations in the center of the track are theoretically relatively well understood. One important point, however, is puzzling as will be discussed in the following.

In Fig. 6 no dependence of the electron temperature on the target structure (amorphous versus crystalline carbon or diamond-like versus graphite-like bonds) is visible, although low-energy electron transport should be very sensitive to the details of the lattice structure. The macroscopic heat conductivity of these materials is completely different. Heat conduction along the atomic planes of graphite should, e.g., exceed the one of a-C by some orders of magnitude. Thus, we have expected to find much lower electron temperatures for HOPG and higher temperature ratios for the two decay times.

There are two possible explanations for the insensitivity with respect to the type of material. First, the samples might have undergone phase transitions towards the same type of carbon. We see, however, no significant change of electron-induced Auger spectra before and after the irradiation and a clear change of the optical reflectivity was found only for the DLC target (for the a-C target there are indications of plastic deformation but not of phase transformations). Thus, at least a-C and HOPG should have different atomic structures. A second explanation for the insensitivity might be the electron transport itself. Hot electrons in the highly excited track may scatter very similar in the three materials.

Note that we have received preliminary results by Caron and Rothard for electron temperatures in a-C during the final preparation stage of this paper. These temperatures have been determined in a completely different way from the Auger spectra and they are about a factor of two below our results. They are, however, subject to significantly larger uncertainties.

5. Conclusions

The energy dissipation due to fast heavy ions in matter is investigated with special attention on possible material-modification mechanisms. It is shown that the energy loss of fast ions is well understood. The remaining deviations between experimental results and theoretical ab initio results are currently only about 10%. Thus, the prediction of impact-parameter dependent energy losses appears to be no significant source of uncertainties for the explanation of track effects. The same holds true for the comparison of experimental and theoretical probabilities for multiple inner-shell ionization. For very heavy ions these results indicate that the center of the track is completely ionized, including the carbon K-shell electrons.

Hence, the main unsolved question concerning material modifications by fast ions is "How are

electronic excitations converted into atomic motion?". In this work we have presented the electron spectroscopy results for different modifications of carbon, i.e.,

- crystalline graphite (HOPG);
- graphite-like a-C (with atomic H fractions of $<10\%$);
- DLC;
- PP – $[C_3H_6]_n$.

For the latter material, we have found high nuclear-track potentials and extremely high-erosion yields with a threshold behavior. Both facts are strong indications for the Coulomb explosion mechanism, a mutual repulsion of highly ionized atoms. For the other target materials high electron temperatures have been found and Coulomb explosion can definitely be excluded. These electron temperatures may lead to material modifications via the electron–phonon coupling (thermal-spike model) or via the modified inter-atomic forces (lattice-relaxation model). So far, it is not possible to distinguish between the latter two energy-conversion mechanisms on a pure experimental basis. From the present work, however, it becomes clear that the pathways for material modifications by fast heavy ions (Coulomb explosion versus thermal spike) are strongly dependent on the type of material.

Acknowledgements

This work was partially supported by CNPq, by the Alexander-von-Humboldt foundation, and through the PROBRAL contract between DAAD and CAPES.

References

[1] R.L. Fleischer, P.B. Price, R.M. Walker, in: Nuclear Tracks in Solids, University of California Press, Berkley, CA, 1975.
[2] R. Spohr, in: Ion Tracks and Microtechnology, F. Vieweg und Sohn Verlagsgesellschaft, Braunschweig, 1990.
[3] S. Klaumünzer, Ming-dong. Hou, G. Schumacher, Phys. Rev. Lett. 57 (1986) 850.
[4] R.E. Johnson, W.L. Brown, Nucl. Instr. and Meth. B 198 (1982) 103.
[5] A. Akkermann, J. Levinson, D. Ilberg, Y. Lifshitz, in: R. Baragiola (Ed.), Ionization of Solids by Heavy Particles, NATO Advanced Study Institutes Series 306, Plenum, New York, 1992, p. 431.
[6] D. Leseur, A. Dunlop, Radiat. Eff. Def. Solids 126 (1993) 163.
[7] C.C. Watson, T.A. Tombrello, Radiat. Eff. 89 (1985) 263.
[8] P. Stampfli, K.H. Bennemann, Phys. Rev. B 49 (1994) 7299.
[9] P. Stampfli, Nucl. Instr. and Meth. B 107 (1996) 138.
[10] F. Desauer, Z. Phys. 12 (1923) 38.
[11] I.M. Lifshitz, M.I. Kaganov, L.V. Tanatarov, J. Nucl. Energy A 12 (1960) 69.
[12] R.H. Ritchie, C. Claussen, Nucl. Instr. and Meth. B 198 (1982) 133.
[13] Z.G. Wang, C. Dufour, E. Paumier, M. Toulemonde, J. Phys.: Condens. Matter 6 (1994) 6733.
[14] G. Szenes, Nucl. Instr. and Meth. B 116 (1996) 141.
[15] A.E. Volkov, V.A. Borodin, Nucl. Instr. and Meth. B 107 (1996) 172.
[16] R.D. Birkhoff, in: S. Flügge (Ed.), Handbuch der Physik, Vol. 34, Springer, Berlin, 1958, p. 53.
[17] M. Rösler, W. Brauer, D. Hasselkamp, in: Particle Induced Electron Emission, Springer Tracts of Modern Physics, Vols. 123 and 123, Springer, Berlin, 1991.
[18] G. Schiwietz, in: R. Baragiola (Ed.), Ionization of Solids by Heavy Particles, NATO Advanced Study Institutes Series 306, Plenum, New York, 1992, p. 197.
[19] H. Rothard, Scanning Microscopy 9 (1995) 1.
[20] G. Schiwietz, P.L. Grande, Nucl. Instr. and Meth. B 69 (1992) 10.
[21] P.L. Grande, G. Schiwietz, Phys. Rev. A 47 (1993) 1119.
[22] G. Schiwietz, P.L. Grande, Radiat. Eff. Def. Solids 130–131 (1994) 137, and references therein.
[23] G. Schiwietz, P.L. Grande, C. Auth, H. Winter, A. Salin, Phys. Rev. Lett. 72 (1994) 2159.
[24] P.L. Grande, G. Schiwietz, Phys. Rev. A 58 (1998) 3796.
[25] G. Schiwietz, P.L. Grande, Nucl. Instr. and Meth. B 153 (1999) 1.
[26] G. de M. Azevedo, P.L. Grande, G. Schiwietz, Nucl. Instr. and Meth. B 164–165 (2000) 203.
[27] The casp code for the UCA and PCA energy-loss theory may be downloaded from http://www.hmi.de/people/schiwietz/casp.html.
[28] P. Sigmund, Nucl. Instr. and Meth. B 135 (1998) 1.
[29] A. Schinner, P. Sigmund, World Scientific, in press.
[30] Extensive energy-loss tabulations are presented by H. Paul at http://www2.unilinz.ac.at/fak/TNF/atomphys/STOPPING/welcome.htm.
[31] H. Geissel, GSI report 82-12, ISSN:0171-4546, Darmstadt, Germany, 1982.
[32] G. Xiao, Ph.D. Thesis, ISBN 3-928943-85-5, Freie Universitaet, Berlin, 1996.
[33] G. Schiwietz, G. Xiao, Private communication.
[34] J.F. Ziegler, J.P. Biersack, U. Littmark, in: The Stopping and Range of Ions in Solids, Pergamon, New York, 1985.

[35] G. Schiwietz, G. Xiao, P.L. Grande, E. Luderer, R. Pazirandeh, U. Stettner, Nucl. Instr. and Meth. B 146 (1998) 131.
[36] G. Schiwietz, G. Xiao, P.L. Grande, E. Luderer, R. Pazirandeh, U. Stettner, Europhys. Lett. 47 (1999) 384.
[37] G. Schiwietz, G. Xiao, E. Luderer, P.L. Grande, Nucl. Instr. and Meth. B 164–165 (2000) 353.
[38] G. Schiwietz, P.L. Grande, B. Skogvall, J.P. Biersack, R. Köhrbrück, K. Sommer, A. Schmoldt, P. Goppelt, I. Kádár, S. Ricz, U. Stettner, Phys. Rev. Lett. 69 (1992) 628.
[39] G. Schiwietz, G. Xiao, Nucl. Instr. and Meth. B 107 (1996) 113.
[40] G. Schiwietz, D. Schneider, J.P. Biersack, N. Stolterfoht, D. Fink, A. Mattis, B. Skogvall, H. Altevogt, V. Montemayor, U. Stettner, Phys. Rev. Lett. 61 (1988) 2677.
[41] D. Schneider, G. Schiwietz, D. DeWitt, Phys. Rev. A 47 (1992) 3945.
[42] G. Xiao, G. Schiwietz, P.L. Grande, A. Schmoldt, N. Stolterfoht, M. Grether, R. Köhrbrück, A. Spieler, U. Stettner, Phys. Rev. Lett. 79 (1997) 1821.
[43] K. Wien, Ch. Koch, Nguyen van Tan, Nucl. Instr. and Meth. B 100 (1995) 322.
[44] G. Galli, R.M. Martin, R. Car, M. Parrinello, Phys. Rev. B 42 (1990) 7470.
[45] J. Schäfer, J. Ristein, R. Graupner, L. Ley, U. Stephan, Th. Frauenheim, V.S. Veerasamy, G.A.J. Amaratunga, M. Weiler, H. Erhardt, Phys. Rev. B 53 (1996) 7762.
[46] C. Kittel, Introduction in Solid-State Physics, Vol. 7, Oldenburg, München, 1988.
[47] E. Knoesel, A. Hotzel, T. Hertel, M. Wolf, G. Ertl, Surf. Sci. 368 (1996) 76.
[48] M. Aeschlimann, M. Bauer, S. Pawlik, Chem. Phys. 205 (1996) 127.
[49] S. Tougaard, P. Sigmund, Phys. Rev. B 25 (1982) 4452.